Supplementary material to: "How macromolecules' softness affects diffusion under crowding"

Edyta Słyk,[1,2] Tomasz Skóra,[1] and Svyatoslav Kondrat[1,3,4,5]

[1] *Institute of Physical Chemistry, Polish Academy of Sciences, 01-224 Warsaw, Poland*

[2] *Department of Theoretical Chemistry, Institute of Chemical Sciences, Faculty of Chemistry, Maria Curie-Skłodowska University in Lublin, 20-031 Lublin, Poland*

[3] *Max-Planck-Institut für Intelligente Systeme, Heisenbergstraße 3, 70569 Stuttgart, Germany*

[4] *IV. Institut für Theoretische Physik, Universität Stuttgart, Pfaffenwaldring 57, 70569 Stuttgart, Germany*

[5] *Institut für Computerphysik, Universität Stuttgart, Allmandring 3, 70569 Stuttgart, Germany*

CONTENTS

S1. MODELS OF MACROMOLECULES

A. Soft and hard particles

We modeled both hard and soft particles with single spheres of hydrodynamic radii $a_{\mathrm{H}} = 5.1\,\mathrm{nm}$, which is equal to the hydrodynamic radius of Ficoll70 – a popular polymer crowding agent [1]. The spheres differ in their hard core (a_{c}) and entanglement (a_{e}) radii. For hard particles $a_{\mathrm{c}} = a_{\mathrm{e}} = a_{\mathrm{H}}$, whereas for soft particles a_{c} and a_{e} are symmetrically splitted around the a_{H} value. Our aim is to single out the effect of softness, so we picked soft particles' a_{c} and a_{e} provide the effective occupied volume equal to hard particle's:

$$v_{\mathrm{occ}} = 4\pi \int_0^\infty r^2(1 - \exp[-\beta U(r; a_{\mathrm{c}}, a_{\mathrm{e}}, U_0)])dr = \frac{4}{3}\pi a_{\mathrm{H}}^3, \tag{S1}$$

where $U(r)$ stands for the interaction potential, which depends, apart from a_{c} and a_{e}, on the parameter U_0 tuning the strength of the shoulder (see Section S1 C). To parametrize our soft particles for given U_0, we solved eq. (S1) for a_{c} and a_{e} with the bisection method, keeping the position of the CESP potential fixed at $a_{\mathrm{c}} + a_{\mathrm{e}} = 2a_{\mathrm{H}}$. We used $a_{\mathrm{H}} = 5.1\,\mathrm{nm}$ as for the hard particle.

All the relevant parameters are gathered in table S1.

TABLE S1. Interaction parameters for hard and soft particles mixtures

	a_{c} (nm)	a_{e} (nm)	βU_0	a_{H} (nm)
hard	5.1	5.1	1.2	5.1
soft	3.35	6.85	1.2	5.1
hard	5.1	5.1	0.8	5.1
soft	2.5	7.7	0.8	5.1

B. IgG and DNA

We used a dsDNA model introduced in our previous publication [2]. It consists of 8 linearly bound identical beads of hydrodynamic radius $a_{\mathrm{bead}} = 1.14\,\mathrm{nm}$ each, with the har-

monic potential on bonds and angles. The Young modulus was $H = 9.866\,\mathrm{kcal\,mol^{-1}\,nm^{-2}}$ and the force constant for angles $12.086\,\mathrm{kcal\,mol^{-1}\,rad^{-2}}$.

Every base pair has electric charge of $2e$, thus in 16-nm dsDNA the total charge sums up to $96e$. For such highly charged molecules the DLVO theory is only valid upon renormalizing the molecular bare charges [3]. We used the renormalization factor 0.2 as in previous studies [4, 5]. The diffusion coefficient was obtained by performing simulations of a single dsDNA which gives $D_{\mathrm{DNA}} = 58 \pm 1.4\,\mathrm{nm^2\,\mu s^{-1}}$. The hydrodynamic radius was calculated from the Stokes-Einstein equation and amounts to $a_{\mathrm{DNA}} = 3.70 \pm 0.09\,\mathrm{nm}$.

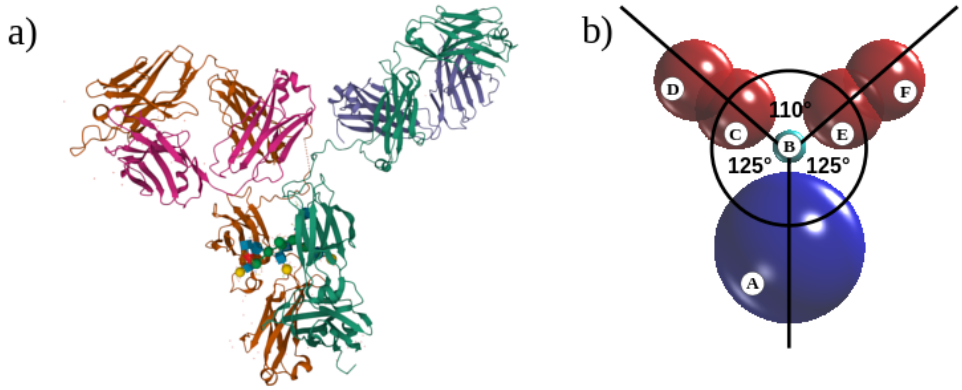

FIG. S1. **IgG molecule** (**a**) Crystal structure of human IgG [6] taken from Protein Data Bank (`http://www.rcsb.org/`, PDB ID: 1HZH) [7] and visualized using Mol* Viewer [8]. (**b**) The IgG model used in this work [9].

We used the model for IgG that we introduce in our upcoming work [9]. Briefly, it consists of six uncharged beads (fig. S1). The interaction parameters between various beads are presented in Tables S2 and S3. The diffusion coefficient and the hydrodynamic radius were calculated in the same way as described above for dsDNA and amount to $D_{\mathrm{IgG}} = 37 \pm 1.0\mathrm{nm^2\,\mu s^{-1}}$ and $a_{\mathrm{IgG}} = 5.8\,\mathrm{nm} \pm 0.2\,\mathrm{nm}$.

C. Interaction potentials

The total interaction potential is constructed by summing four contributions – WCA potential (U_{WCA}), CESP potential (U_{CESP}), DLVO electrostatic potential (U_{DLVO}), and bonded

TABLE S2. Sizes of the subunits of IgG particle.

Subunit	$a_{\mathrm{H}} = a_{\mathrm{c}} = a_{\mathrm{e}}$ (nm)
A	4.5
B	1.0
C	2.42
D	2.42
E	2.42
F	2.42

TABLE S3. Values of equilibrium bond length and equilibrium angle used in IgG model.

Subunit	Bond length (nm)	Force constant ($\mathrm{kcal\,mol^{-1}\,nm^{-2}}$)
A - B	6.0	1909.86595
B - C		
B - E	3.9	1909.86595
C - D		
E - F	3.0	1909.86595
Subunit	**Angle value**	**Force constant ($\mathrm{kcal\,mol^{-1}\,rad^{-2}}$)**
A - B - C	125.0°	0.05
A - B - E	125.0°	0.05
B - C - D	180.0°	10.00
B - E - F	180.0°	10.00
C - B - E	110.0°	0.05

potential (U_{bonded}):

$$U = U_{\mathrm{WCA}} + U_{\mathrm{CESP}} + U_{\mathrm{DLVO}} + U_{\mathrm{bonded}}. \tag{S2}$$

For systems composed of hard and soft spheres only, U_{DLVO} and U_{bonded} are both zero.

1. WCA repulsion

We included repulsive interactions between any pairs of particles, excluding however the the IgG beads belonging to the same macromolecule and dsDNA beads that are directly

connected by a bond. The interaction potential [10]

$$U_{\mathrm{WCA}}\left(r_{ij}\right)=\frac{\epsilon_{\mathrm{WCA}}\pi^{2}}{315}\left(\frac{a_{i}a_{j}}{a_{i}+a_{j}}\right)\frac{\sigma^{6}}{\left[r_{ij}-\left(a_{i}+a_{j}\right)\right]^{7}}. \tag{S3}$$

To ensure that all van der Waals atoms fit inside the macromolecules, we decreased the hard core radii by a value equal to the radius of van der Waals atom ($\sigma = 0.15\,\mathrm{nm}$)

$$a_{i}\mapsto a_{i}^{*}=a_{i}-\sigma. \tag{S4}$$

We used a lower and an upper cut-off for the distance between pairs of particles, as follows. For particles with surface-to-surface separation below 0.08 nm, the repulsive force was assumed constant (and equal to the value at the 0.08 nm separation). This is done in order to avoid numerical problems due to large forces (note the strong divergence of eq. (S3) at $r_{ij} = a_i + a_j$). The upper cutoff for computing (numerically) WCA interactions was set to $r_{ij}^{(max)} = 15\,\mathrm{nm}$, i.e., we set $U_{\mathrm{WCA}}(r_{ij} \geq r_{ij}^{(max)}) = 0$.

Finally, we note that for all the pairs of particles for which U_{WCA} is relevant we have used $\epsilon_{\mathrm{WCA}} = 0.37\,\mathrm{kcal\,mol^{-1}}$. This choice follows ref. 4, which successfully reproduced the *in vivo* diffusion coefficient of the green fluorescent protein (GFP) in a complex model of cytoplasm by using the ϵ_{WCA} value quoted above.

2. CESP repulsion

In order to account for the softness of macromolecules, we used Chain-Entanglement Softened Potential (CESP) introduced by Blanco *et al.* [11]:

$$U_{\mathrm{CESP}}\left(r_{ij}\right)=\frac{U_{0}}{2}\left[1-\tanh\left(\frac{\mathfrak{a}a_{\mathrm{c}}}{a_{\mathrm{e}}-a_{\mathrm{c}}}(r_{ij}-[a_{\mathrm{e}}+a_{\mathrm{c}}])\right)\right], \tag{S5}$$

where a_{c} is the hard-core radius, U_0 describes the magnitude of the entanglement interactions, and a_{e} – their extension. $\mathfrak{a}$ sets the length scale (we set $\mathfrak{a} = 1\,\mathrm{nm^{-1}}$ in all calculations in line with ref. 11). For the interaction between a hard and a soft particle, we took the same U_0 as for two soft particles. a_{c} and a_{e} are obtained *via* Lorentz combining rule (see table S1). For interactions between hard particles, $a_{\mathrm{e}} = a_{\mathrm{c}}$, hence the contribution from U_{CESP} is zero.

3. Electrostatic repulsion

We modeled the electrostatic repulsion between nonconnected dsDNA beads using the DLVO (Derjaguin, Landau, Verwey and Overbeek) electrostatic potential [12]:

$$U_{\mathrm{DLVO}}\left(r_{ij}\right) = \frac{\Theta_i \Theta_j e^2}{4\pi\varepsilon_0\varepsilon\left(1+\kappa a_i\right)\left(1+\kappa a_j\right)} \frac{\exp\left[-\kappa\left(r_{ij}-a_i-a_j\right)\right]}{r_{ij}}, \tag{S6}$$

where κ ($= 1.039\,25\,\mathrm{nm}^{-1}$) denotes inverse of the Debye screening length, e – elementary electric charge, $\varepsilon = 78.54$ – the relative dielectric constant, ε_0 – vacuum permittivity, and Θ_i – bead's charge. We used a cutoff for electrostatic interactions equal to 25 nm.

4. Bonded interactions

The bonded potential consists of bond and angle components. We used the bond potential as implemented in BD_BOX:

$$\begin{aligned} U_{\mathrm{bonded}}\left(r_{ij}; H, r_{\mathrm{eq}}, r_{\max}\to\infty\right) = \\ -\frac{1}{2}Hr_{\max}^2 \ln\left(\frac{r_{\max}^2 - r_{ij}^2}{r_{\max}^2 - r_{\mathrm{eq}}^2}\right) - \frac{1}{2}Hr_{\max}r_{\mathrm{eq}} \ln\left[\frac{\left(r_{\max}+r_{ij}\right)\left(r_{\max}-r_{\mathrm{eq}}\right)}{\left(r_{\max}-r_{ij}\right)\left(r_{\max}+r_{\mathrm{eq}}\right)}\right], \end{aligned} \tag{S7}$$

where r_{eq} is the equilibrium bond length, $r_{\max}$ is the maximum bond length and H – the force constant. By setting very large $r_{\max}$ ($r_{\max} = 2\,500\,000.0\,\mathrm{nm}$) it converges to standard harmonic potential:

$$U_{\mathrm{bonded}}\left(r_{ij}; H, r_{\mathrm{eq}}, r_{\max}\to\infty\right) = \frac{1}{2}H\left(r_{ij}-r_{\mathrm{eq}}\right)^2. \tag{S8}$$

We used the angle potential as implemented in BDBOX:

$$U_{\mathrm{bonded}}\left(\alpha_{ijk}; \xi, \alpha_{\mathrm{eq}}\right) = \frac{1}{2}\xi\left(\alpha_{ijk}-\alpha_{\mathrm{eq}}\right)^2, \tag{S9}$$

where ξ is the angle force constant and α_{eq} – the equilibrium angle value. The values of force constants and equilibrium bond lengths/angles are gathered in table S3.

S2. BROWNIAN DYNAMICS SIMULATIONS

We used a customized version of the simulation package BD_BOX [13] (see `https://www.fuw.edu.pl/~mdlugosz/downloads.html`). The modification included the Lennard-Jones and soft (CESP) interactions between all types of "macromolecules". Brownian dynamics trajectories have been generated by using the second order Iniesta-de la Torre algorithm [14, 15] where the position of ith bead at time t is

$$r_i = r_i^0 + \frac{1}{2}\frac{\Delta t}{k_B T}\sum_{j=1}^{N}\left(\boldsymbol{D}_{ij}^0 \boldsymbol{F}_j^0 + \boldsymbol{D}'_{ij}\boldsymbol{F}'_j\right) + \boldsymbol{R}_i, \tag{S10}$$

where N is the number of beads, $\Delta t = t - t_0 > 0$ is the time step, r_i^0 is the position of the ith bead at time t_0, k_B is the Boltzmann constant and T temperature. The (position-dependent) diffusion matrix $\boldsymbol{D}_{ij}^0$ (see Section S2 A) and the force $\boldsymbol{F}_j^0$ acting on the jth bead are evaluated at time t_0, while $\boldsymbol{D}'_{ij}$ and $\boldsymbol{F}'_j$ are evaluated for beads in a configuration with the positions at an intermediate corrector step [14].

The $3N$-dimensional vector of random displacements, $\hat{\boldsymbol{R}} = \{\boldsymbol{R}_i\} = \hat{\boldsymbol{B}}\hat{\boldsymbol{X}}$, where $\hat{\boldsymbol{X}}$ is a random Gaussian vector, and matrix $\hat{\boldsymbol{B}} = \{\boldsymbol{B}_{ij}\}$ is a 'square root' of the diffusion tensor, *i.e.*,

$$\hat{\boldsymbol{D}} = \hat{\boldsymbol{B}}\hat{\boldsymbol{B}}^T \tag{S11}$$

where $\hat{\boldsymbol{D}} = \{\boldsymbol{D}_{ij}\}$. For the Iniesta-de la Torre algorithm, the diffusion matrix used in eq. (S11) is $(\hat{\boldsymbol{D}}^0 + \hat{\boldsymbol{D}}')/2$, so that the random forces satisfy

$$\langle \boldsymbol{R}_i \rangle = 0, \quad \langle \boldsymbol{R}_i \boldsymbol{R}_j^T \rangle = \Delta t \left(\boldsymbol{D}_{ij}^0 + \boldsymbol{D}'_{ij}\right). \tag{S12}$$

We used Cholesky decomposition to calculate $\hat{\boldsymbol{B}}$, as implemented in BD_BOX, which we performed every 100 steps to increase the performance, similarly as in ref. 2, 4, 16.

A. Hydrodynamic interactions

We used the generalized Rotne-Prager-Yamakawa tensor [17–19], which reads (a_i is the bead's hydrodynamic radius, r_{ij} the center-to-center separation between the i'th and j'th beads, η is viscosity, and $\boldsymbol{I}$ is the unit tensor):

$$\boldsymbol{D}_{ii} = \frac{k_B T}{6\pi\eta a_i}\boldsymbol{I}; \tag{S13a}$$

$$\boldsymbol{D}_{ij}(r_{ij}) = \frac{k_B T}{8\pi\eta r_{ij}} \left[\left(1 + \frac{a_i^2 + a_j^2}{3r_{ij}^2} \right) \boldsymbol{I} + \left(1 - \frac{a_i^2 + a_j^2}{r_{ij}^2} \right) \frac{r_{ij} r_{ij}^T}{r_{ij}^2} \right] \tag{S13b}$$

for $r_{ij} > a_i + a_j$;

$$\boldsymbol{D}_{ij}(r_{ij}) = \frac{k_B T}{8\pi\eta r_{ij}} \left[\frac{16 r_{ij}^3 (a_j + a_j) - [(a_i - a_j)^2 + 3r_{ij}^2]^2}{32 r_{ij}^3} \boldsymbol{I} + \frac{3[(a_i - a_j)^2 - r_{ij}^2]^2}{32 r_{ij}^3} \frac{r_{ij} r_{ij}^T}{r_{ij}^2} \right] \tag{S13c}$$

for $a_{ij}^M - a_{ij}^m < r_{ij} < a_i + a_j$, where a_{ij}^M is the largest and a_{ij}^m the smallest of a_i and a_j; and

$$\boldsymbol{D}_{ij} = \frac{k_B T}{6\pi\eta a_{ij}^M} \boldsymbol{I}, \tag{S13d}$$

for $r_{ij} < a_{ij}^M - a_{ij}^m$.

B. Simulation parameters

The box size was 85 nm × 85 nm × 85 nm and periodic boundary conditions were applied in all three directions. In order to account for the long-range character of the hydrodynamic interactions, we used the Ewald summation [20], as implemented in BD_BOX [13]. The parameter controlling the convergence of the Ewald summation was $\sqrt{\pi}$ (default value in BD_BOX). The maximal magnitude of both real and reciprocal lattice vectors was 2. For computational efficiency, the diffusion tensor was updated once per 100 steps [2, 4, 16] (each update causes the Cholesky decomposition).

In all simulations, the temperature was $T = 298.15\,\mathrm{K}$ (room temperature) and the viscosity of the medium (need for the computation of the hydrodynamic interactions) $\eta = 1.02\,\mathrm{cP}$, corresponding to water.

The time step Δt (eq. (S10)) was 0.5 ps; a BD simulation runs for at least 2×10^7 iterations steps, i.e., a total time of at least 10 µs.

C. Simulated systems

The number of particles for the occupied volume fractions and molar fractions simulated in this work are presented in tables S4 and S5.

TABLE S4. Studied hard and soft particles mixtures

Volume fraction	Molar fraction		Particle number	
	hard	soft	hard	soft
10 %	0.28	0.72	31	80
10 %	0.72	0.28	81	30
10 %	1.00	0.00	111	0
10 %	0.00	1.00	0	111
30 %	1.00	0.00	333	0
30 %	0.00	1.00	0	333

TABLE S5. Studied IgG/DNA and hard/soft particles mixtures

Volume fraction	Molar fraction		Particle number	
	IgG/DNA	hard/soft	IgG/DNA	hard/soft
		IgG		
10 %	0.28	0.72	30	79
		DNA		
10 %	0.25	0.75	36	107

D. Trajectory analysis and MSD

Ensemble-averaged mean-square displacement (MSD) is

$$\mathrm{MSD}(m\Delta t) = \frac{1}{N_{\mathrm{traj}}} \sum_{i=1}^{N_{\mathrm{traj}}} \{r_i\,[m\Delta t] - r_i\,[0]\}^2. \tag{S14}$$

However, to gather more statistics, we used time-averaged MSD (TAMSD), which should lead to the same results in the long-time limit. As in our previous work [2, 16], we used FREUD library [21] to calculate TAMSD

$$\mathrm{TAMSD}(m\Delta t) = \frac{1}{N_{\mathrm{traj}}} \sum_{i=1}^{N_{\mathrm{traj}}} \frac{1}{N_{\mathrm{steps}} - m} \sum_{k=0}^{N_{\mathrm{steps}}-m-1} \{r_i\,[(k+m)\Delta t] - r_i\,[k\Delta t]\}^2, \tag{S15}$$

where N_{traj} is the number of trajectories and N_{steps} the total number of steps. The shift Δt in trajectory analysis was 5 ns.

The time-dependent relative apparent diffusion coefficient is:

$$\frac{D(t)}{D_0} = \frac{\mathrm{TAMSD}(t)}{6D_0 t}, \tag{S16}$$

where D_0 is diffusion coefficient in infinite dilution. For a spherical particle, D_0 is given by the Stokes-Einstein equation.

The long-time diffusion coefficients D_l have been obtained by fitting to a constant the numerical results for $\frac{D(t)}{D_0}$ in a time window around $t = 5\,\mu\mathrm{s}$. Uncertainty of the simulation results due to sampling error was estimated by dividing the simulations into 5 subsets and treating them as independent 'measurements'.

S3. MONTE CARLO SIMULATIONS

To compute the occupied and excluded volume fractions in our simulation systems (based on snapshots from BD simulations), we used Monte Carlo (MC) insertion method presented below.

1. The positions of the particles are loaded from the selected BD snapshot.
2. The *tracer* is thrown into the system at a randomly generated position (and orientation for dsDNA and IgG).
3. The tracer potential energy V_i is computed.
4. Counting variable x is incremented by $1 - \exp\left(-V_\mathrm{i}/k_\mathrm{B}T\right)$.
5. The tracer is removed from the system.
6. Steps 2-5 are repeated N times.
7. After N repeats, the value $\frac{x}{N}$ is taken as an estimate of the excluded volume fraction.

For hard-sphere potential, the method is equivalent to incrementing x only in the case of overlap. Note that for a single particle and the same tracer, the calculated volume fractions are related to the second virial coefficient [22]

$$B_2 = 2\pi \int_0^\infty dr r^2 \left[1 - e^{-V/k_\mathrm{B}T}\right]. \tag{S17}$$

We also note that the 'effective' hard sphere radius $a_{\mathrm{B}_2} = (3B_2/2\pi)^{1/3}$ that follows from B_2 differs from the 'equivalent' hard-core diameter defined by Barker and Henderson [23]

$$2a_\mathrm{equ} = \int_0^\infty dr \left[1 - e^{-V/k_\mathrm{B}T}\right], \tag{S18}$$

which amounts to $a_\mathrm{equ} = 4.8\,\mathrm{nm}$ and $a_\mathrm{equ} = 4.2\,\mathrm{nm}$ for $U_0 = 1.2k_\mathrm{B}T$ and $0.8k_\mathrm{B}T$, respectively.

Excluded volumes for various pairs of particles are shown in table S6. The excluded volumes for the simulated systems of hard and soft particles are presented in tables S7 and S8.

TABLE S6. Volume excluded by a single hard/soft particle to another hard/soft particle expressed as a multiple of hard particle volume v_H.

	$v_\mathrm{ex}(H-H)$	$v_\mathrm{ex}(H-S)$	$v_\mathrm{ex}(S-S)$
$\beta U_0 = 0.8$			
$a_\mathrm{c} = 2.5\,\mathrm{nm}$			
$a_\mathrm{e} = 7.7\,\mathrm{nm}$	$8v_\mathrm{H}$	$6.14v_\mathrm{H}$	$5.85v_\mathrm{H}$
$\beta U_0 = 1.2$			
$a_\mathrm{c} = 3.35\,\mathrm{nm}$			
$a_\mathrm{e} = 6.85\,\mathrm{nm}$	$8v_\mathrm{H}$	$7.20v_\mathrm{H}$	$6.92v_\mathrm{H}$

TABLE S7. Excluded volume fractions in simulated systems of occupied volume fraction $\phi_\mathrm{occ} = 10\,\%$ composed of soft particles ($\beta U_0 = 1.2$, $a_\mathrm{c} = 3.35\,\mathrm{nm}$, $a_\mathrm{e} = 6.85\,\mathrm{nm}$) and hard particles ($a_\mathrm{c} = a_\mathrm{e} = 5.1\,\mathrm{nm}$).

$\phi_\mathrm{occ} = 10\,\%$, $\beta U_0 = 1.2$			
Tracer	$x_\mathrm{soft} = 100\,\%$	$x_\mathrm{soft} = 73\,\%$	$x_\mathrm{soft} = 27\,\%$
$a_\mathrm{c} = 0\,\mathrm{nm}$			
$a_\mathrm{e} = 0\,\mathrm{nm}$	$9.90 \pm 0.02\%$	$9.95 \pm 0.03\%$	$9.99 \pm 0.03\%$
$a_\mathrm{c} = 5.1\,\mathrm{nm}$			
$a_\mathrm{e} = 5.1\,\mathrm{nm}$	$56.2 \pm 0.5\%$	$58.9 \pm 0.7\%$	$61.1 \pm 0.7\%$
$a_\mathrm{c} = 3.35\,\mathrm{nm}$			
$a_\mathrm{e} = 6.85\,\mathrm{nm}$	$54.4 \pm 0.4\%$	$56.1 \pm 0.6\%$	$57.3 \pm 0.5\%$

TABLE S8. Excluded volume fractions in simulated systems of occupied volume fraction $\phi_{\mathrm{occ}} = 30\,\%$ composed of soft particles ($\beta U_0 = 1.2$, $a_{\mathrm{c}} = 3.35\,\mathrm{nm}$, $a_{\mathrm{e}} = 6.85\,\mathrm{nm}$) and hard particles ($\beta U_0 = 1.2$, $a_{\mathrm{c}} = 5.1\,\mathrm{nm}$, $a_{\mathrm{e}} = 5.1\,\mathrm{nm}$).

$\phi_{\mathrm{occ}} = 30\,\%$, $\beta U_0 = 1.2$		
Tracer	$x_{\mathrm{soft}} = 100\,\%$	$x_{\mathrm{soft}} = 0\,\%$
$a_{\mathrm{c}} = 0\,\mathrm{nm}$		
$a_{\mathrm{e}} = 0\,\mathrm{nm}$	$27.6 \pm 0.2\%$	$30.1 \pm 0.10\%$
$a_{\mathrm{c}} = 5.1\,\mathrm{nm}$		
$a_{\mathrm{e}} = 5.1\,\mathrm{nm}$	$95.4 \pm 0.12\%$	$99.1 \pm 0.2\%$
$a_{\mathrm{c}} = 3.35\,\mathrm{nm}$		
$a_{\mathrm{e}} = 6.85\,\mathrm{nm}$	$94.0 \pm 0.14\%$	$98.1 \pm 0.3\%$

S4. SUPPLEMENTARY PLOTS

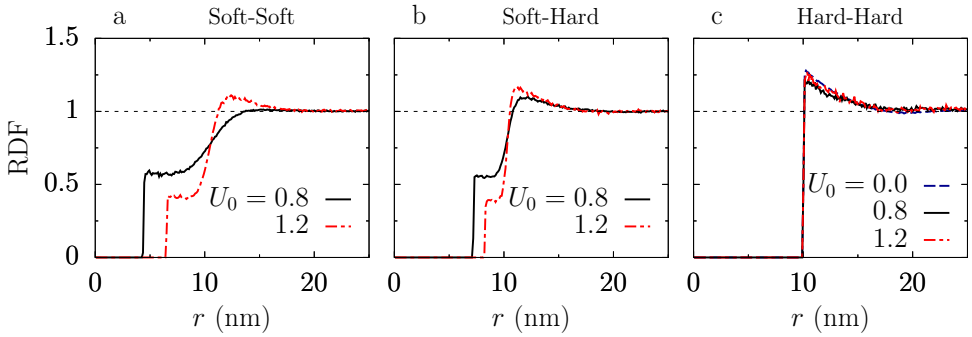

FIG. S2. **Radial distribution functions (RDFs).** RDFs between various crowders for different parameters of the softened shoulder potential (eq. (1) in the main text) in a mixture of soft and hard (Ficoll70) crowders. Occupied volume fraction $\phi_{\mathrm{occ}} = 10\,\%$ and the fraction of hard particles $x_{\mathrm{hard}} \approx 27\,\%$.

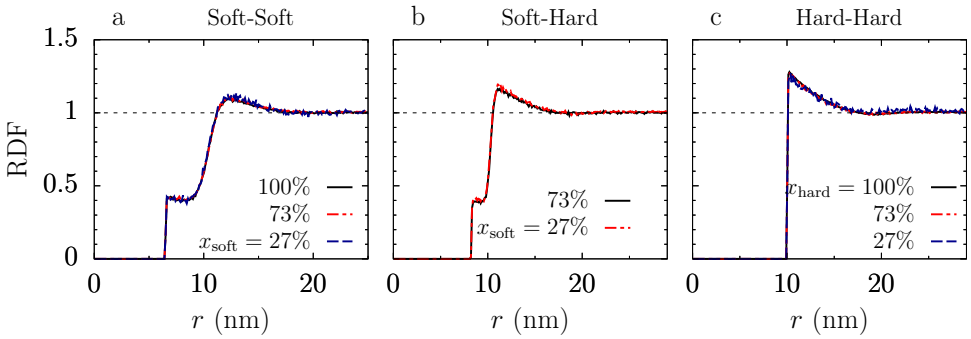

FIG. S3. **Radial distribution functions (RDFs).** RDFs between various crowders for different molar fractions of the soft crowders in a mixture of soft and hard crowders. Occupied volume fraction $\phi_{\mathrm{occ}} = 10\,\%$.

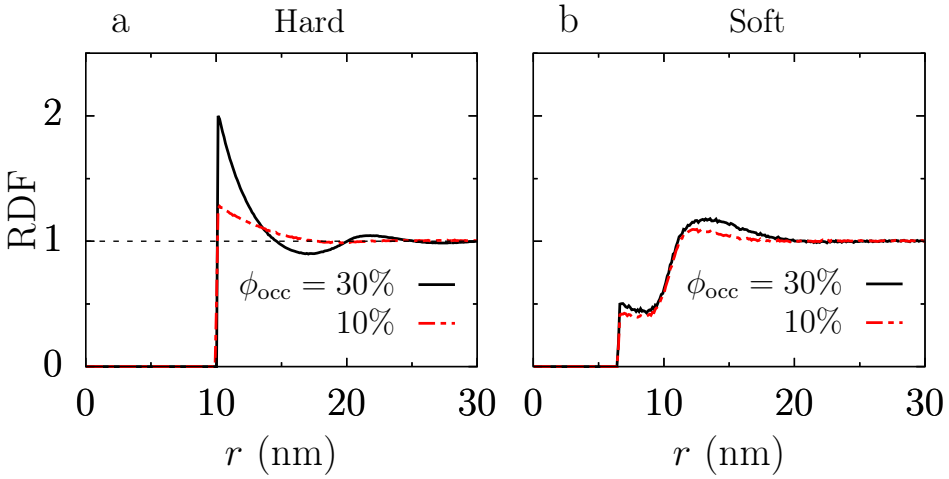

FIG. S4. **Radial distribution functions (RDFs).** RDFs between hard and soft crowders in unmixed systems for two occupied volume fractions ϕ_{occ}.

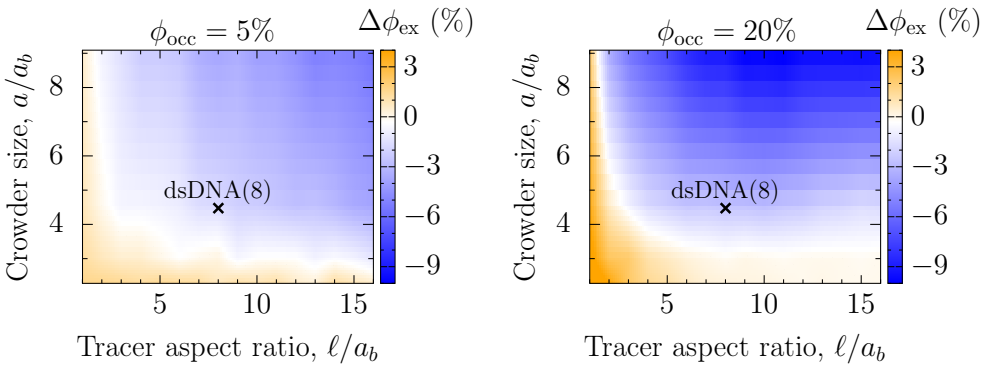

FIG. S5. **Volume fractions excluded to a dsDNA by soft and hard crowders.** Difference in the excluded volume fractions $\Delta\phi_{\mathrm{ex}} = \phi_{\mathrm{ex}}^{\mathrm{hard}} - \phi_{\mathrm{ex}}^{\mathrm{soft}}$ for a rigid polymer of length ℓ (modelling dsDNA pieces) in hard and soft crowders of the same hydrodynamic radius a_{H}. a_b is the radius of a polymer bead.

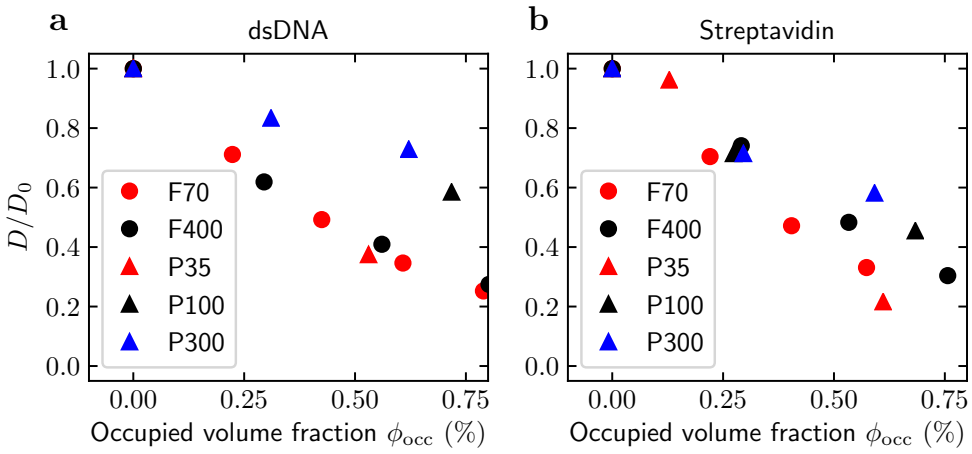

FIG. S6. **Translational diffusion of dsDNA and Streptavidin tracers in solutions of various crowding agents.** The results are taken from ref. 1. These authors calculated the occupied volume fractions ϕ_{occ} using the measured mass of crowders and specific volumes of Ficoll and PEG/PEO ($0.65\,mL\,g^{-1}$ and $0.83\,mL\,g^{-1}$, respectively) [1]. To match with our results, we computed ϕ_{occ} from the hydrodynamic radii and molecular masses, assuming that all crowders are spheres of the size determined by the hydrodynamic radius. Note that while this is likely a reasonable approximation for Ficoll, the physical (gyration) radius of a soft crowder (PEG/PEO) is larger. We *assume*, however, that the *effective* radius is equal to the hydrodynamic radius in the sense used in this work (see fig. 1 in the main text). The specific volumes computed with this strategy are between an order and two orders of magnitude larger than used in ref. 1, namely: $4.78\,mL\,g^{-1}$ (Ficoll70), $6.30\,mL\,g^{-1}$ (Ficoll400), $13.34\,mL\,g^{-1}$ (PEG35), $28.36\,mL\,g^{-1}$ (PEO100), $46.05\,mL\,g^{-1}$ (PEO200), and $61.37\,mL\,g^{-1}$ (PEO300). The hydrodynamic radii are 5.1 nm (Ficoll70), 10 nm (Ficoll400), 5.7 nm (PEG35), 10.4 nm (PEO100), 15.4 nm (PEO200), and 19.4 nm (PEO300).

[1] N. O. Junker, F. Vaghefikia, A. Albarghash, H. Höfig, D. Kempe, J. Walter, J. Otten, M. Pohl, A. Katranidis, S. Wiegand, and J. Fitter, Impact of Molecular Crowding on Translational Mobility and Conformational Properties of Biological Macromolecules, J. Phys. Chem. B **123**, 4477 (2019).

[2] T. Skóra, F. Vaghefikia, J. Fitter, and S. Kondrat, Macromolecular Crowding: How Shape

and Interactions Affect Diffusion, J. Phys. Chem. B **124**, 7537 (2020).

[3] Y. Levin, Electrostatic correlations: from plasma to biology, Reports Prog. Phys. **65**, 1577 (2002).

[4] T. Ando and J. Skolnick, Crowding and hydrodynamic interactions likely dominate in vivo macromolecular motion, Proc. Natl. Acad. Sci. **107**, 18457 (2010).

[5] S. Kondrat, O. Zimmermann, W. Wiechert, and E. von Lieres, The effect of composition on diffusion of macromolecules in a crowded environment, Phys. Biol. **12**, 046003 (2015).

[6] E. O. Saphire, P. W. Parren, R. Pantophlet, M. B. Zwick, G. M. Morris, P. M. Rudd, R. A. Dwek, R. L. Stanfield, D. R. Burton, and I. A. Wilson, Crystal structure of a neutralizing human IgG against HIV-1: A template for vaccine design, Science (80-.). **293**, 1155 (2001).

[7] H. M. Berman, J. Westbrook, Z. Feng, G. Gilliland, T. N. Bhat, H. Weissig, I. N. Shindyalov, and P. E. Bourne, The Protein Data Bank, Nucleic Acids Res. **28**, 235 (2000).

[8] D. Sehnal, S. Bittrich, M. Deshpande, R. Svobodová, K. Berka, V. Bazgier, S. Velankar, S. K. Burley, J. Koča, and A. S. Rose, Mol* Viewer: modern web app for 3D visualization and analysis of large biomolecular structures, Nucleic Acids Res. **49**, W431 (2021).

[9] E. Słyk, T. Skóra, and S. Kondrat, A minimal coarse-grained model for Immunoglobulin G (IgG): Diffusion and binding under crowding, , in preparation (2022).

[10] D. Henderson, D.-M. Duh, X. Chu, and D. Wasan, An expression for the dispersion force between colloidal particles, J. Colloid Interface Sci. **185**, 265 (1997).

[11] P. M. Blanco, J. L. Garcés, S. Madurga, and F. Mas, Macromolecular diffusion in crowded media beyond the hard-sphere model, Soft Matter **14**, 3105 (2018).

[12] J. N. Israelachvili, *Intermolecular and Surface Forces* (IOP Publishing, 2015) p. 1577.

[13] M. Długosz, P. Zieliński, and J. Trylska, Brownian dynamics simulations on CPU and GPU with BD-BOX, J. Comput. Chem. **32**, 2734 (2011).

[14] A. Iniesta and J. García de la Torre, A second-order algorithm for the simulation of the Brownian dynamics of macromolecular models, J. Chem. Phys. **92**, 2015 (1990).

[15] M. Długosz and J. Trylska, Diffusion in crowded biological environments: Applications of Brownian dynamics, BMC Biophys. **4**, 3 (2011).

[16] T. Skóra, M. N. Popescu, and S. Kondrat, Conformation-changing enzymes and macromolecular crowding, Phys. Chem. Chem. Phys. **23**, 9065 (2021).

[17] J. Rotne and S. Prager, Variational Treatment of Hydrodynamic Interaction in Polymers, J.

Chem. Phys. **50**, 4831 (1969).

[18] H. Yamakawa, Transport properties of polymer chains in dilute solution: hydrodynamic interaction, J. Chem. Phys. **53**, 436 (1970).

[19] P. J. Zuk, E. Wajnryb, K. A. Mizerski, and P. Szymczak, Rotne-Prager-Yamakawa approximation for different-sized particles in application to macromolecular bead models, J. Fluid Mech. **741**, R5 (2014).

[20] E. R. Smith, I. K. Snook, and W. Van Megen, Hydrodynamic interactions in Brownian dynamics, Phys. A Stat. Mech. its Appl. **143**, 441 (1987).

[21] V. Ramasubramani, B. D. Dice, E. S. Harper, M. P. Spellings, J. A. Anderson, and S. C. Glotzer, freud: A software suite for high throughput analysis of particle simulation data, Comput. Phys. Commun. **254**, 107275 (2020), arXiv:1906.06317.

[22] M. G. Noro and D. Frenkel, Extended corresponding-states behavior for particles with variable range attractions, J. Chem. Phys. **113**, 2941 (2000).

[23] J. A. Barker and D. Henderson, What is "liquid"? Understanding the states of matter, Rev. Mod. Phys. **48**, 587 (1976).